Contrast enhancement using silica microspheres in coherent anti-Stokes Raman spectroscopic imaging

Xi Huang, N. He X., Wei Xiong, Yang Gao, Li Jia Jiang, Lei Liu, Yun Shen Zhou, Lan Jiang, Jean-François Silvain, Yongfeng Lu

▶ **To cite this version:**

Xi Huang, N. He X., Wei Xiong, Yang Gao, Li Jia Jiang, et al.. Contrast enhancement using silica microspheres in coherent anti-Stokes Raman spectroscopic imaging. Optics Express, 2014, 22 (3), pp.2889-2896. 10.1364/OE.22.002889 . hal-00956572

HAL Id: hal-00956572
https://hal.science/hal-00956572

Submitted on 7 May 2024

HAL is a multi-disciplinary open access archive for the deposit and dissemination of scientific research documents, whether they are published or not. The documents may come from teaching and research institutions in France or abroad, or from public or private research centers.

L'archive ouverte pluridisciplinaire **HAL**, est destinée au dépôt et à la diffusion de documents scientifiques de niveau recherche, publiés ou non, émanant des établissements d'enseignement et de recherche français ou étrangers, des laboratoires publics ou privés.

Distributed under a Creative Commons Attribution - NonCommercial - NoDerivatives 4.0 International License

Contrast enhancement using silica microspheres in coherent anti-Stokes Raman spectroscopic imaging

X. Huang,[1] X. N. He,[1] W. Xiong,[1] Y. Gao,[1] L. J Jiang,[1] L. Liu,[1] Y. S. Zhou,[1] L. Jiang,[2] J. F. Silvain,[3] and Y. F. Lu[1,*]

[1]*Department of Electrical Engineering, University of Nebraska-Lincoln, Lincoln, Nebraska 68588-0511, USA*
[2]*School of Mechanical Engineering, Beijing Institute of Technology, 100081, China*
[3]*Institut de Chimie de la Matière Condensée de Bordeaux – ICMCB-CNRS 87, Avenue du Docteur Albert Schweitzer F-33608 Pessac Cedex, France*
[*]*ylu2@unl.edu*

Abstract: Coherent anti-Stokes Raman scattering (CARS) microscopy is a powerful imaging technique that can provide chemical information of organic and nonorganic materials through vibrational spectroscopy. However, its contrast is not sufficient for monitoring thin film materials. In this study, silica microspheres were employed for enhancing the signal contrast in CARS imaging. One layer of optically transparent silica microspheres was self-assembled onto polymer grating samples to enhance the CARS signals. The highest contrast enhancement factor of 12.5 was achieved using 6.1-μm-diameter microspheres. Finite-difference time-domain method (FDTD) simulation was conducted to simulate the contrast enhancement with silica microspheres of different diameters.

©2014 Optical Society of America

OCIS codes: (300.0300) Spectroscopy; (300.6230) Spectroscopy, coherent anti-Stokes Raman scattering; (300.6450) Spectroscopy, Raman.

References and links

1. C. L. Evans and X. S. Xie, "Coherent anti-Stokes Raman scattering microscopy: chemical imaging for biology and medicine," Annu. Rev. Anal. Chem. **1**(1), 883–909 (2008).
2. C. L. Evans, E. O. Potma, M. Puoris'haag, D. Côté, C. P. Lin, and X. S. Xie, "Chemical imaging of tissue in vivo with video-rate coherent anti-Stokes Raman scattering microscopy," Proc. Natl. Acad. Sci. U. S. A. **102**(46), 16807–16812 (2005).
3. G. W. H. Wurpel, J. M. Schins, and M. Müller, "Chemical specificity in three-dimensional imaging with multiplex coherent anti-Stokes Raman scattering microscopy," Opt. Lett. **27**(13), 1093–1095 (2002).
4. X. S. Xie, J. Yu, and W. Y. Yang, "Living cells as test tubes," Science **312**(5771), 228–230 (2006).
5. T. B. Huff, Y. Z. Shi, W. J. Sun, W. Wu, R. Shi, and J. X. Cheng, "Real-time CARS imaging reveals a calpain-dependent rathway for paranodal myelin retraction during high-frequency stimulation," PLoS ONE **6**, e17176 (2011).
6. R. F. Begley, A. B. Harvey, and R. L. Byer, "Coherent anti-Stokes Raman spectroscopy," Appl. Phys. Lett. **25**(7), 387–390 (1974).
7. C. L. Evans, E. O. Potma, and X. S. Xie, "Coherent anti-Stokes Raman scattering spectral interferometry: determination of the real and imaginary components of nonlinear susceptibility $\chi(3)$ for vibrational microscopy," Opt. Lett. **29**(24), 2923–2925 (2004).
8. F. Ganikhanov, C. L. Evans, B. G. Saar, and X. S. Xie, "High-sensitivity vibrational imaging with frequency modulation coherent anti-Stokes Raman scattering (FM CARS) microscopy," Opt. Lett. **31**(12), 1872–1874 (2006).
9. A. Zumbusch, G. R. Holtom, and X. S. Xie, "Three-dimensional vibrational imaging by coherent anti-Stokes Raman scattering," Phys. Rev. Lett. **82**(20), 4142–4145 (1999).
10. M. Hashimoto, T. Araki, and S. Kawata, "Molecular vibration imaging in the fingerprint region by use of coherent anti-Stokes Raman scattering microscopy with a collinear configuration," Opt. Lett. **25**(24), 1768–1770 (2000).
11. S. H. Parekh, Y. J. Lee, K. A. Aamer, and M. T. Cicerone, "Label-free cellular imaging by broadband coherent anti-Stokes Raman scattering microscopy," Biophys. J. **99**(8), 2695–2704 (2010).

#201161 - $15.00 USD Received 12 Nov 2013; revised 23 Jan 2014; accepted 27 Jan 2014; published 31 Jan 2014
(C) 2014 OSA

12. T. T. Le, H. M. Duren, M. N. Slipchenko, C. D. Hu, and J. X. Cheng, "Label-free quantitative analysis of lipid metabolism in living Caenorhabditis elegans," J. Lipid Res. **51**(3), 672–677 (2010).
13. X. L. Nan, J. X. Cheng, and X. S. Xie, "Vibrational imaging of lipid droplets in live fibroblast cells with coherent anti-Stokes Raman scattering microscopy," J. Lipid Res. **44**(11), 2202–2208 (2003).
14. X. N. He, J. Allen, P. N. Black, T. Baldacchini, X. Huang, H. Huang, L. Jiang, and Y. F. Lu, "Coherent anti-Stokes Raman scattering and spontaneous Raman spectroscopy and microscopy of microalgae with nitrogen depletion," Biomed. Opt. Express **3**(11), 2896–2906 (2012).
15. K. König, H. Liang, M. W. Berns, and B. J. Tromberg, "Cell damage in near-infrared multimode optical traps as a result of multiphoton absorption," Opt. Lett. **21**(14), 1090–1092 (1996).
16. Y. Fu, H. Wang, R. Shi, and J. X. Cheng, "Characterization of photodamage in coherent anti-Stokes Raman scattering microscopy," Opt. Express **14**(9), 3942–3951 (2006).
17. E. O. Potma, X. S. Xie, L. Muntean, J. Preusser, D. Jones, J. Ye, S. R. Leone, W. D. Hinsberg, and W. Schade, "Chemical imaging of photoresists with Coherent Anti-Stokes Raman Scattering (CARS) microscopy," J. Phys. Chem. B **108**(4), 1296–1301 (2004).
18. H. Kano and H. Hamaguchi, "Ultrabroadband (>2500 cm^{-1}) multiplex coherent anti-Stokes Raman scattering microspectroscopy using a supercontinuum generated from a photonic crystal fiber," Appl. Phys. Lett. **86**(12), 121113 (2005).
19. G. W. H. Wurpel, J. M. Schins, and M. Müller, "Chemical specificity in three-dimensional imaging with multiplex coherent anti-Stokes Raman scattering microscopy," Opt. Lett. **27**(13), 1093–1095 (2002).
20. J. X. Cheng, A. Volkmer, L. D. Book, and X. S. Xie, "Multiplex coherent anti-Stokes Raman scattering microscopy and study of lipid vesicles," J. Phys. Chem. B **106**(34), 8493–8498 (2002).
21. W. Xiong, Y. S. Zhou, X. N. He, Y. Gao, M. Mahjouri-Samani, L. Jiang, T. Baldacchini, and Y. F. Lu, "Simultaneous additive and subtractive three-dimensional micro/nano-fabrication using integrated two-photon polymerization and multi-photon ablation," Light Sci. Appl. **1**, e6 (2012).
22. H. Wang, K. K. Mendu, Y. F. Lu, J. Shi, D. R. Alexander, and D. W. Doerr, "Laser-assisted fabrication of 3-D structures on polymer film," J. Laser Micro Nanoeng. **1**(2), 106–110 (2006).
23. Z. B. Wang, W. Guo, L. Li, B. Luk'yangchuk, A. Khan, Z. Liu, Z. C. Chen, and M. H. Hong, "Optical virtual imaging at 50nm lateral resolution with a white-light nanoscope," Nat. Commun. **2**, 218 (2011).
24. K. J. Yi, H. Wang, Y. F. Lu, and Z. Y. Yang, "Enhanced Raman scattering by self-assembled silica spherical microparticles," J. Appl. Phys. **101**(6), 063528 (2007).
25. Z. G. Chen, A. Taflove, and V. Backman, "Photonic nanojet enhancement of backscattering of light by nanoparticles: a potential novel visible-light ultramicroscopy technique," Opt. Express **12**(7), 1214–1220 (2004).
26. B. G. Saar, C. W. Freudiger, J. Reichman, C. M. Stanley, G. R. Holtom, and X. S. Xie, "Video-rate molecular imaging in vivo with stimulated Raman scattering," Science **330**(6009), 1368–1370 (2010).

1. Introduction

During the last decade, coherent anti-Stokes Raman scattering (CARS) microscopy has become a powerful tool for vibrational imaging of chemical and biological samples [1–5]. It has been proven that CARS [6–9] is more sensitive than spontaneous Raman spectroscopy due to extreme lower typical photon conversion efficiencies in Raman scattering [10,11]. CARS involves the interaction of four waves designated as pump (p), Stokes (s), probe (p'), and anti-Stokes, where pump and probe waves are usually fixed to the same frequency ($\omega_\rho = \omega_{\rho'}$). When the beat frequency between the pump and the Stokes beams is matched with the resonant vibrational frequency Ω_R of molecules or lattices of samples, a resonant enhancement of the third-order nonlinear optical process occurs and greatly promotes the sensitivity with chemical selectivity. The higher-order dependence on laser power makes CARS more sensitive than spontaneous Raman spectroscopy, which can provide fast contrast imaging based on the intrinsic molecular vibrations of a specimen without the need for extrinsic labels [11–14] and has been demonstrated to be particularly sensitive to lipid-rich structures based on the resonant CARS signals from the C-H vibration [12–14]. However, the CARS contrast is not sufficiently high for monitoring or imaging thin films. There is also a nonresonant contribution to the CARS signals from the sample that does not carry chemically specific information [6–8], which can distort and overwhelm the resonant signals of interest. Simply increasing the excitation laser power increases the risk of multiphoton damage to the samples [15,16]. A research from Xie's group was reported that single frequency CARS microscopy can successfully be used to monitor thin photoresists used in photolithography, which could perform imaging subtraction to suppress the non-resonance background [17]. However, this method could not be applied to a broadband CARS microscope. In this study,

#201161 - $15.00 USD Received 12 Nov 2013; revised 23 Jan 2014; accepted 27 Jan 2014; published 31 Jan 2014
(C) 2014 OSA

we have achieved a high contrast of CARS by employing silica microspheres in a broadband CARS microscope. The test samples chosen here were polymer grating samples fabricated by two-photon polymerization (TPP) lithography, because of their CH-rich periodic line pattern and simple fabrication process. One layer of optically transparent silica microspheres of 3 ~7 μm in diameter were self-assembled on the polymer grating samples consisting of 400-nm-wide lines spaced 280 nm apart to achieve high-contrast grating images in CARS imaging, as shown in Fig. 1.

2. Experimental methods

2.1 CARS experimental setup

Broadband CARS microscopy [18–20] based on a photonic crystal fiber light source has been considered to be a simpler solution for CARS microscopy than the complex picosecond laser and optical parametric oscillator (OPO) systems. Figure 2 shows a schematic of the broadband CARS microscope. Both the pump and Stokes beams are provided by a single fs laser (MaiTai DeepSee HP, SpectraPhysics) in conjunction with a supercontinuum generator (SCG).The SCG ensures that broadband anti-Stokes signals at different frequencies can be obtained without tuning the laser wavelength. As shown in Fig. 2, the mode-locked Ti:Sapphire fs laser provides a laser beam with a fixed wavelength of 800 nm, whose typical duration, power, and repetition are 100 fs, 2.95 W, and 80 MHz, respectively. The laser was isolated from the rest of the setup by a Faraday isolator and divided into two beams by a beam splitter to form the pump and Stokes beams. A 50/50 ultrafast beam splitter designed for S-polarization was used. The splitting ratio was controlled by a ½ λ waveplate which rotated the input polarization. Each arm of the setup had a variable attenuator, allowing independent control of the laser power. The Stokes beam was formed using a ~500 mW laser to generate the supercontinuum in the SCG and then filtering the beam through a long-pass filter (RG830, Newport). The other 800 nm beam passed through an attenuator and was guided to a delay line. Two laser pulses were superimposed collinearly using an 800-nm Notch filter and then tightly focused onto the samples using an Olympus objective (1.05 NA, × 25) in an upright laser scanning microscope (LSM). Under the tight focusing condition, the phase-matching condition is relaxed due to the large angular dispersion and small interaction volume [1,12,20]. The laser powers for the pump and the broadband Stokes lasers before entering the microscope are 40 and 60 mW, respectively. The bandpass filter used for CARS imaging was a Semrock FF01-650/13 (T_{avg}>93% @643.5~656.5 nm, center wavelength = 650 nm, and bandwidth = 13 nm). The substrates used for the forward CARS imaging were 0.17-mm-thick glass slides. Finally, the CARS signal was detected by a photomultiplier (PMT) inside the LSM.

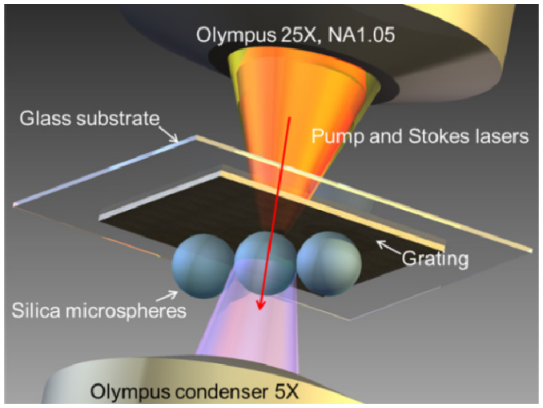

Fig. 1. Experimental configuration of contrast-enhanced CARS imaging using the transmission-mode broadband CARS microscopy integrated with an assembly of silica microspheres.

#201161 - $15.00 USD Received 12 Nov 2013; revised 23 Jan 2014; accepted 27 Jan 2014; published 31 Jan 2014
(C) 2014 OSA

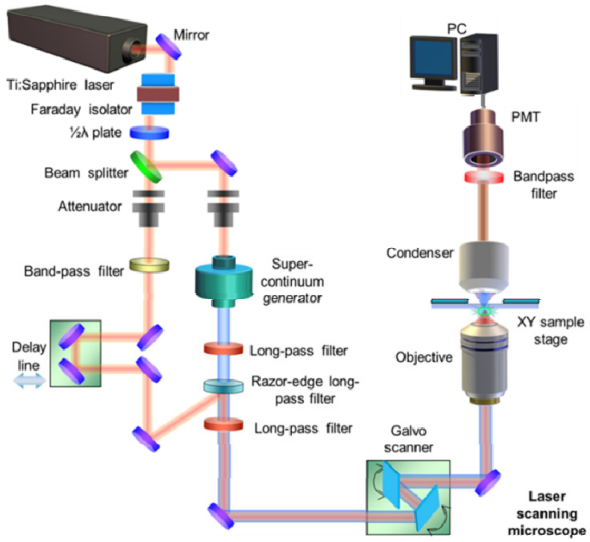

Fig. 2. Schematic of the setup of the broadband forward CARS imaging system.

2.2 Fabrication of grating samples and self-assembly of silica microspheres

The grating fabrication process consisted of two steps. First, TPP lithography [21] was employed to fabricate the grating samples using a negative photoresist (IP-L from Nanoscribe GmbH). Second, unsolidified photoresist was washed away by rinsing the sample in isopropyl alcohol for 20 min. The laser beam for the TPP process was generated by a mode-lock fs fiber laser (780 nm central wavelength, 100 MHz repetition rate, and 120 fs pulse duration). The laser power used in the grating fabrication was ~4 mW and the writing speed is set to 60 μm/s. The laser beam was tightly focused within the IP-L photoresist by an oil-immersion objective lens (1.4 NA, × 100). The grating consists of 400-nm-wide lines spaced 280 nm apart, as shown in Fig. 3(a). The thickness of the polymer sample is ~500 nm. Several monodisperse suspensions of 1% diluted SiO_2 microspheres of 3~7 μm in diameter (Bangs Laboratories) were used to self-assemble an ordered monolayer of microspheres on the grating surface by drop coating [22]. The substrates were tilted with an angle about 40 degrees to the base during the drop coating and then dried on the air. The SEM image of grating structure assembled by 6.1 μm silica microspheres is shown in Fig. 3(b). The Raman spectrum of the IP-L photoresist [Fig. 3(b)] shows a strong Raman peak at around 2800~3000 cm^{-1}, which correlated to the C-H group vibration. CARS is also sensitive to the same C-H vibrational signatures as seen in Raman spectroscopy. However, unlike Raman spectroscopy, the CARS signal is detected on the blue side of the incoming 800 nm pump laser. Therefore, the CARS signals for the C-H vibrational signatures in the wavelength unit were 645~657 nm, so the 650/13 nm bandpass filter was chosen for CARS C-H imaging.

#201161 - $15.00 USD Received 12 Nov 2013; revised 23 Jan 2014; accepted 27 Jan 2014; published 31 Jan 2014
(C) 2014 OSA

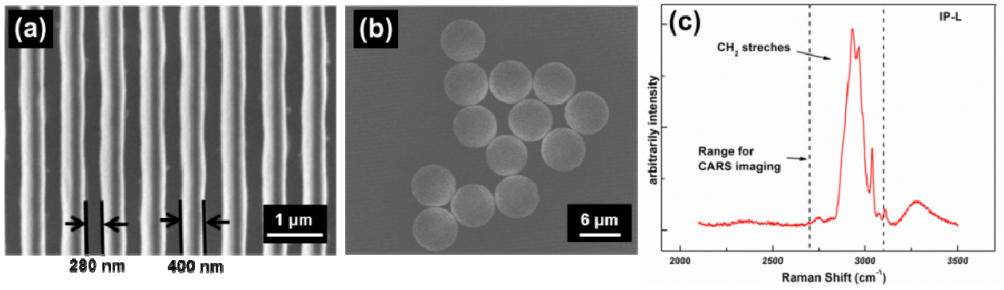

Fig. 3. (a) SEM image of the grating structure (400-nm-wide lines spaced 280 nm apart), (b) SEM image of 6.1 μm silica microspheres, and (c) Raman spectrum of the IP-L photoresist (excited by 514 nm Ar^+ laser). The range for CARS CH imaging is due to the 650/13 nm bandpass filter used in the experiment.

3. Results and discussion

3.1 Contrast-enhanced CARS imaging of grating samples using silica microspheres with different diameters

Silica microspheres with five different diameters (3.13, 3.92, 5.06, 6.1, and 6.46 μm) were employed to study the size dependence of the contrast-enhanced CARS imaging. In the experiment, the grating with microspheres was reversely placed in the upright LSM. The collinear pump and Stokes pulse were tightly focused on the grating to generate the CARS signals, which went through the microspheres and were enhanced. The enhancement in CARS imaging was observed for all samples, and only the signals of those grating lines with microspheres were enhanced in the CARS imaging.

As can be seen from Fig. 4(a), only those lines above the microspheres have been enhanced. The lines without silica microspheres show a low CARS contrast, which cannot be easily distinguished due to the low CARS contrast. The intensity profiles in Figs. 4(b) and 4(c) show the enhanced intensity when using the 6.1-μm-diameter microspheres. Moreover, the 3D intensity profile in Fig. 4(d) allows us to distinguish the grating more easily. Although the silica microspheres would have a non-resonant background in CARS imaging, the silica microspheres do not have any active Raman bands in 2000 cm^{-1} ~3000 cm^{-1} range. In the experiment, we observed that if there were no grating lines with the microspheres, no enhanced line pattern could be observed. Therefore, the enhanced line pattern is from the polymer grating rather than the silica microspheres. The diameter of the microspheres used here was 6.1 μm, but the view window in the circle [Fig. 4(a)] was only ~4 μm in diameter, showing 4~5 enhanced lines. It may result from the enhanced effect, which can only affect a small area very close to the microspheres' surface. It is also noted that the focal planes for imaging the grating lines with/without microspheres should be the same, because the lasers were focused on the grating and scanned in the same focal plane by a galvo scanner in the LSM. Moreover, the 3D CARS image [Fig. 5(e)] shows that the enhancement happened in 3D space using 5.06-μm-diameter microspheres, considering an ~1 μm depth of laser interaction volume. The 3D image was formed by Z-stacks of the 2D section images. The four 2D (x-y plane) images shown in Figs. 5(a)–5(d) were acquired at various depths in the Z axis with a 1 μm step. It means that even the grating lines were out of focus (focus plane is at Z = 2 μm), the microspheres can enhance weak CARS signals produced by the laser interaction with the volume edge, which are filtered out by the 650/13nm bandpass filter and imaged by the PMT in the LSM. Here, the enhanced area by the 5.06 μm microspheres is smaller than that of the 6.1 μm ones, which shows 3~4 enhanced lines.

#201161 - $15.00 USD Received 12 Nov 2013; revised 23 Jan 2014; accepted 27 Jan 2014; published 31 Jan 2014
(C) 2014 OSA

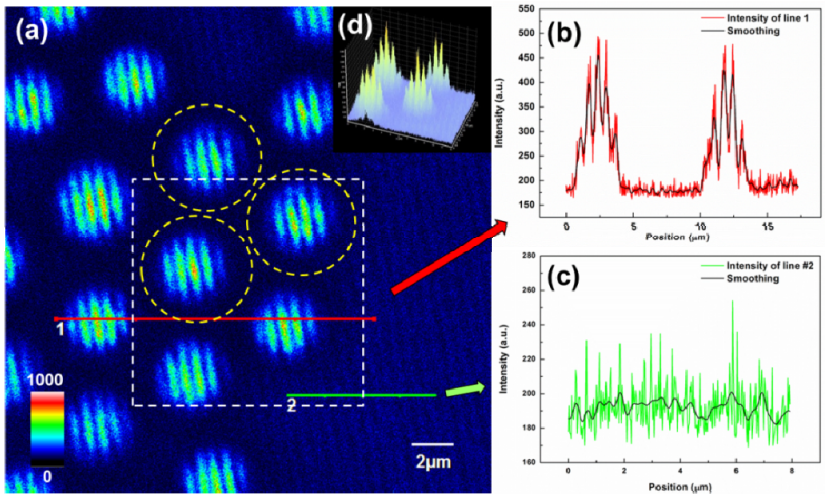

Fig. 4. (a) Enhanced CARS imaging of the grating using 6.1 μm silica microspheres. (b),(c) shows the intensity profile of indicator lines 1 and 2 in (a), respectively. (d). 2D intensity profile of the white area shown in (a).

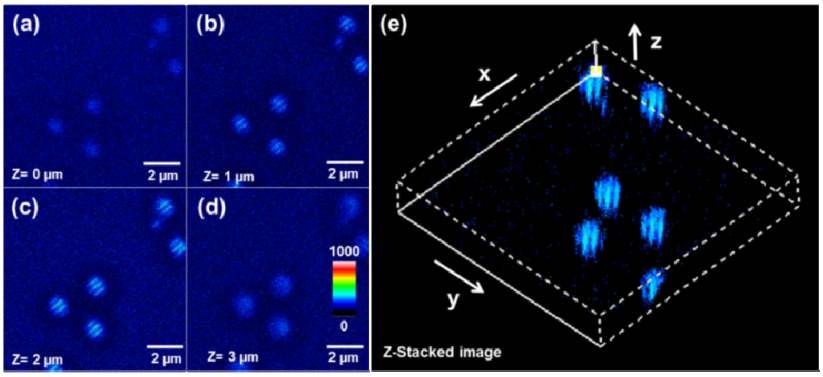

Fig. 5. (a)-(d) 2D CARS images at various Z depths and (e) 3D Z-stacked image (z = 0~3 μm) of the grating (located at z = 2.0 μm) assembled with the 5.06 μm microspheres.

The enhance factor (EF) has also been evaluated by the following equation:

$$EF = \frac{CNR'}{CNR} = \frac{(I_{A'} - I_{B'})}{(I_A - I_B)}, \quad (1)$$

where *CNR'* and *CNR* are the contrast-to-noise ratio for CARS imaging with and without microspheres, respectively. $I_{A'}$ and $I_{B'}$ are the signal intensity for the signal producing structure A (line) and B (no line) in the view region of the microspheres, and I_A and I_B are the signal intensity for structures A and B outside the view region of the microspheres. It was found that the EFs for 6.1 μm and 5.06 microspheres are 12.5 and 5.47 times, respectively.

3.2 FDTD simulation of optical fields with silica microspheres below the grating

In this study, FDTD algorithm under perfectly matched layer boundary conditions was used to simulate the optical field using Optiwave™. The microspheres were simulated as pure silica, whose refractive index was set to 1.45. The pulsed laser sources used in the experiments were fs pulsed lasers with a high repetition rate of 80 MHz, so the CARS signals from the C-H vibrations in the anti-Stokes frequency could be generated by tightly focusing the pump and Stokes lasers. Point sources were assumed to simulate the CARS signals of

#201161 - $15.00 USD Received 12 Nov 2013; revised 23 Jan 2014; accepted 27 Jan 2014; published 31 Jan 2014
(C) 2014 OSA

650 nm since the width of grating line is ~400 nm. The lighting lines can be considered as point sources because of the similar size compared to the CARS nonlinear resolution. The magnitude of the E-field of the CARS signals was assumed to be 1 V m^{-1}. The uniform mesh step for each axis was 40 nm. Figures 6(a) and 6(b) show the E-field distribution in a 2D view with and without a microsphere. It is known that microspheres can generate "photonic nanojets" with super small foci [23–25]. However, the divergent electromagnetic wave from a small area very close to the microspheres can be confined to a parallel propagation wave with a relatively narrow distribution with smaller full width at half maximum (FWHM) of the CARS signal wave, which increases the detection efficiency and enhance the imaging intensity. Moreover, to quantify the enhancement factor in the simulation, an observation plane was placed in the propagation direction. Figure 6(c) shows the E-field distribution on the observation plane with and without microspheres, which shows that the E-field will have a narrower distribution of CARS signal wave when microspheres are applied. The narrower FWHM indicates the higher detection intensity, as shown in Fig. 7. All the microspheres (3.13, 3.92, 5.06, 6.1, and 6.46 μm) result in the enhancment of CARS contrast in the experiment. The EFs are caculated by Eq. (1). The strongest EF occurs when a 6.1 μm microsphere is applied. While in the simulation, the narrowest FWHM occurs with a 6 μm microsphere. Thus, the experimental results match the simulation results well.

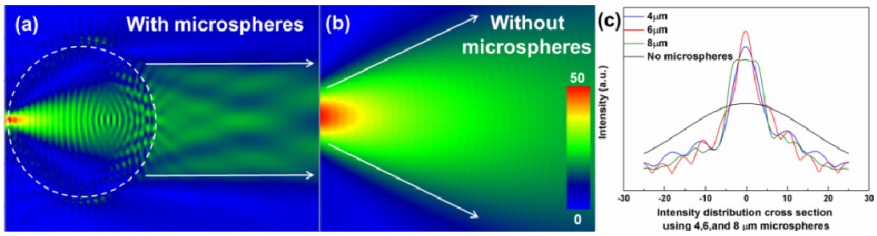

Fig. 6. Calculated distributions of the electric fields under a signal light (650 nm) with (a) and without (b) a microsphere of 6 μm in the XZ cross-section. (c) The calculated E-field distributions on the same observation plane.

4. Conclusions

In summary, one layer of silica microspheres of different diameters was self-assembled onto the polymer grating samples to achieve the contrast-enhanced CARS imaging. The highest contrast enhancement factor of 12.5 was achieved using 6.1 μm microspheres under the polymer grating. The FDTD simulation of the CARS enhancement by the microspheres was also conducted. The optimized size for the microspheres based on simulation is found to be 6 μm for the 650 nm CARS signal of C-H bonds, which has the lowest FWHM of distribution in the direction of propagation and the highest CARS intensity. Thus, by applying silica microspheres, the CARS intensity and contrast can be significantly improved. Moreover, in last years a new coherent Raman imaging technique, stimulated Raman scattering (SRS) microscopy, shows many advantages as compared with CARS [26]. Due to their similar setup, our method could also be used in an SRS configuration.

#201161 - $15.00 USD Received 12 Nov 2013; revised 23 Jan 2014; accepted 27 Jan 2014; published 31 Jan 2014
(C) 2014 OSA

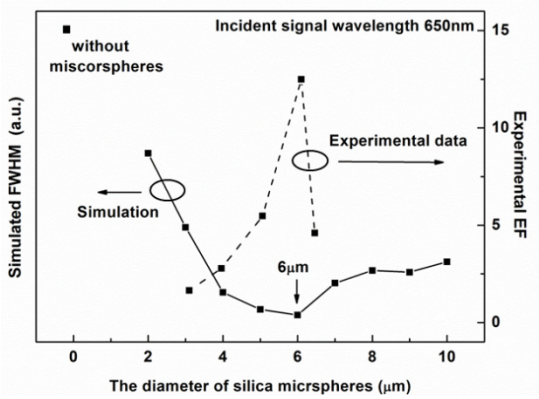

Fig. 7. The simulated FWHM of the CARS signal distributions and the experimental EFs using different diameter microspheres.

Acknowledgment

This research work was financially supported by National Science Foundation (CMMI 1126208 and CMMI-0900419).

#201161 - $15.00 USD Received 12 Nov 2013; revised 23 Jan 2014; accepted 27 Jan 2014; published 31 Jan 2014
(C) 2014 OSA